
Neural mechanisms mediating responses to abutting gratings: Luminance edges vs. illusory contours

YUNING SONG AND CURTIS L. BAKER

McGill Vision Research Unit, Department of Ophthalmology, McGill University, Montréal, Québec, Canada

(RECEIVED August 12, 2005; ACCEPTED December 22, 2005)

Abstract

The discontinuities of phase-shifted abutting line gratings give rise to perception of an “illusory contour” (IC) along the line terminations. Neuronal responses to such ICs have been interpreted as evidence for a specialized visual mechanism, since such responses cannot be predicted from conventional linear receptive fields. However, when the spatial scale of the component gratings (carriers) is large compared to the neuron’s luminance passband, these IC responses might be evoked simply by the luminance edges at the line terminations. Thus by presenting abutting gratings at a series of carrier spatial scales to cat A18 neurons, we were able to distinguish genuine nonlinear responses from those due to luminance edges. Around half of the neurons (both simple and complex types) showed a bimodal response pattern to abutting gratings: one peak at a low carrier spatial frequency range that overlapped with the luminance passband, and a second distinct peak at much higher frequencies beyond the neuron’s grating resolution. For those bimodally responding neurons, the low-frequency responses were sensitive to carrier phase, but the high-frequency responses were phase-invariant. Thus the responses at low carrier spatial frequencies could be understood *via* a linear model, while the higher frequency responses represented genuine nonlinear IC processing. IC responsive neurons also demonstrated somewhat lower spatial preference to the periodic contours (envelopes) compared to gratings, but the optimal orientation and motion direction for both were quite similar. The nonlinear responses to ICs could be explained by the same energy mechanism underlying responses to second-order stimuli such as contrast-modulated gratings. Similar neuronal preferences for ICs and for gratings may contribute to the form-cue invariant perception of moving contours.

Keywords: Illusory contours, Texture segregation, Figure-ground segregation, Visual perception, Receptive field

Introduction

The discontinuities of phase-shifted abutting line gratings (Fig. 1A) give rise to perception of an “illusory contour” (IC) along the line terminations. Such ICs have been of great interest because they have provided a paradigm for studying how visual perception goes beyond the physical image projected on the retina, that is, how the brain fills in the gap between the discrete line terminations and generates a percept of a continuous and concrete contour (perceptual completion, Pessoa et al., 1998).

About half of the sampled neurons in primate V2 have been reported to prefer similar orientations of ICs and of gratings (von der Heydt et al., 1984; von der Heydt & Peterhans, 1989). Since there is no luminance gradient along the IC, a conventional linear receptive field (RF) would fail to signal the orientation of the phase shifts. A series of control experiments further suggested that these IC responses were not simply evoked by the luminance contrasts of the line terminations (von der Heydt

et al., 1984; von der Heydt & Peterhans, 1989). Subsequent studies reported that neurons in cat A18 (Redies et al., 1986; Leventhal et al., 1998; Zhou et al., 2001), primary visual fore-brain of owls (Nieder and Wagner, 1999), and even cells in the optic lobula of insects (Horridge et al., 1992) exhibited similar orientation selectivity for ICs and for luminance bars or simple gratings. Optical imaging studies have also indicated somewhat similar cortical orientation maps for such ICs and for gratings in cat A18 (Sheth et al., 1996) and in monkey V2 (Ramsden et al., 2001; Zhan & Baker, 2004, 2006).

Based on these physiological findings, several models have been used to account for IC responses in visual cortex. Von der Heydt and co-workers (von der Heydt et al., 1984; von der Heydt & Peterhans, 1989) proposed a model in which at least two sets of end-stopped neurons are simultaneously activated (Fig. 1B) by the line terminations. Their outputs are then integrated by a single neuron, which could signal the orientation of the ICs. Wilson (1999) proposed an energy-detection model (filter-rectify-filter [FRF]) to account for IC responses. In this scheme, a nonlinear rectification connects two sets of linear filters, which are selective for the spatial frequencies of the component lines and the ICs, respectively (Fig. 1C).

Address correspondence and reprint requests to: Yuning Song, McGill Vision Research Unit, 687 Pine Avenue West, H4-14, Montréal, Québec, Canada, H3A 1A1. E-mail: yuning.song@mcgill.ca

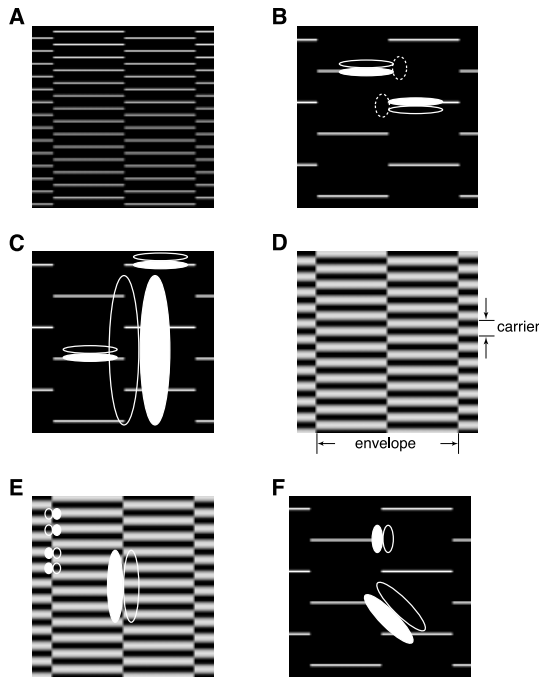


Fig. 1. Abutting grating stimuli and possible neural mechanisms. A and B, an example of an abutting line grating stimulus and a possible role of end-stopped cells. The RF of the end-stopped cell is presented as a conventional linear RF, which has flanking excitatory (white) and inhibitory (black) regions, plus a suppressive end zone (dotted). End-stopped neurons are activated by the line terminations, and their responses are then integrated to signal the orientation of the phase-shifts. C, the FRF. Responses from smaller RFs activated by the horizontal component gratings are rectified and passed on to a larger RF that detects the orientation of the phase shifts. D, an example of an abutting sinewave grating stimulus. A horizontally oriented, high spatial frequency sinewave grating (“carrier”) abruptly changes phase along vertically oriented ICs that occur as a periodic, low spatial frequency (“envelope”) pattern. E, possible linear mechanism accounting for abutting sinewave grating responses. The large linear RF in the middle will give no response since the dark and light regions of the stimulus cancel out within its inhibitory and excitatory zones. However, smaller RFs (upper left) can be activated by the luminance changes at the phase shifts. F, linear RFs could be activated by the luminance contrast at the line terminations, oriented either parallel (top) or obliquely (bottom) to the phase shifts.

Similar IC stimuli can also be constructed from sinewave gratings (Fig. 1D), whose simplicity in the Fourier domain makes them more analytically powerful from a systems analysis point of view. Grosos et al. (1993) reported that neuronal responses in primate V1 to such abutting sinewave gratings were phase-invariant, suggesting that such responses were evoked by the phase shifts along the contour. But whether abutting sinewave gratings could be processed in a similarly nonlinear manner as abutting line gratings remains controversial. Intuitively, one might think that no filling-in process would be needed for detecting abutting sinewave gratings, since each luminance edge along the abutting borders could be sensed by a linear mechanism (Fig. 1E, small cartoon RFs at upper left) (Skottun, 1994; Peterhans, 1997; Nieder, 2002). However, when the spatial frequency of the component grating is sufficiently high compared to the neuron’s RF, the small luminance edges would exceed the resolution of a linear mechanism (Fig. 1E,

large RF). Thus the nature of neural responses to abutting sinewave gratings might be critically dependent on the spatial scale of the stimuli compared to the neuron’s luminance passband.

Other studies suggested that even for abutting line gratings, a filling-in process might not be needed under some circumstances. Using computer simulations, Skottun (1994) demonstrated that drifting abutting line gratings contained Fourier energy components that could potentially activate conventional spatiotemporally linear receptive fields. Single-unit studies also demonstrated that some V1 neurons responded most vigorously to abutting gratings (either line or sinewave) of low but not high spatial frequency component gratings (Peirce & Lennie, 2002). Since low spatial frequency component gratings have more luminance contrast at the line terminations, these responses may have arisen from a linearly summing mechanism (Fig. 1F). Thus a question arises from these studies: are neuronal responses to abutting gratings (both line and sinewave types) driven by the local luminance edges (linear) or by the phase shifts (ICs, nonlinear)? To address this problem, it is important to find a reliable and quantitative method to clarify the linear vs. nonlinear responses.

Abutting gratings share certain features with contrast-modulation stimuli (Zhou & Baker, 1993, 1996; Mareschal & Baker, 1999); that is, both are composed of a relatively high spatial frequency “carrier” that which is modulated by a moving low spatial frequency “envelope” waveform.* Previous studies found that neuronal responses to contrast-modulation stimuli reflected a specialized nonlinear mechanism, since they were selective for high carrier spatial frequencies (e.g. Zhou & Baker, 1993). Here we adopted a similar approach, that is, testing carrier spatial frequency responses, to distinguish global contour responses from local luminance-edge responses. Neurons were tested with a series of phase-shifted abutting gratings in which the spatial scale of the component grating was varied systematically from as low as the neuron’s grating spatial passband to values much higher than the neuron’s grating acuity. If neural responses are evoked by local luminance cues, then the best responses would occur at a similar scale to the neurons’ (relatively low) preferred grating spatial frequency. However neural responses at relatively high spatial frequencies would indicate a nonlinear mechanism.

Our results demonstrated that most neurons responded when the component grating spatial frequencies overlapped the neurons’ luminance passband. These responses were often sensitive to the phase of the component gratings, consistent with a linear mechanism. On the other hand, about half of these neurons also responded to a limited band of high component grating spatial frequencies that were beyond the neurons’ luminance resolution. These responses were phase-invariant, indicating a nonlinear mechanism. We then quantitatively explored the physiological properties of the nonlinear processing. The nonlinear responses to abutting gratings exhibited characteristic tuning to both global and local orientation and spatial frequency, consistent with a multiple-stage processing scheme in which two linear stages are connected by a nonlinear operation (FRF energy model).

*However note that abutting gratings differ from previously used contrast-modulation stimuli in their physical construction (squarewave modulation of phase rather than sinewave modulation of contrast), Fourier power spectra (Zhan & Baker, 2006), perceptual appearance (clearly defined contours rather than fuzzy transparency), and possible luminance-mediated responses (luminance edges along the phase discontinuity rather than distortion products from early nonlinearities in the stimulus or in the retina).

Materials and methods

Animal preparation

Animal preparation was conventional (Mareschal & Baker, 1999)—briefly, cats were first anesthetized with halothane/oxygen, followed by venous cannulation and tracheotomy. Anesthesia was maintained with I.V. thiopentone sodium (2.5%) during surgery and was maintained subsequently with nitrous oxide/oxygen supplemented with I.V. sodium pentobarbital (1 mg/kg-h). A craniotomy was centered on A18 (A3/L4, Horsley-Clark coordinates) for entry of a glass-coated platinum-iridium microelectrode (Frederick Haer). Vital life signs (EEG, EKG, expired CO₂, body temperature) were monitored and maintained throughout the experiment. All animal procedures were approved by the Animal Care Committee of McGill University and were in accordance with the guidelines of the Canadian Council on Animal Care.

Visual stimuli

Visual stimuli were generated by a Macintosh computer (G4, 1 GHz and 1 GB RAM) using Matlab (The Mathworks) with Psychophysics Toolbox software (Brainard, 1997; Pelli, 1997) and displayed at a viewing distance of 57 cm on a gamma-corrected cathode ray tube (CRT) screen (NEC FP1350, 640 × 480, 75 Hz, 36 cd/m²). Examples of abutting line and sinewave gratings are shown in Figs. 1A and D, respectively. The component grating (or inducing grating) will be referred to as the “carrier,” and the profile of its phase modulation will be termed the “envelope.” Abutting sinewave gratings were presented within circular windows surrounded by a uniform gray background of the same mean luminance. Abutting line gratings constructed from white lines were presented against a uniform black background. In both cases, the background luminance was maintained across the entire screen between stimulus presentations and as blank conditions to measure baseline spontaneous activity.

Extracellular recording

Extracellular signals from single units were isolated with a window discriminator and monitored on a delay-triggered digital oscilloscope. A neuron’s receptive field was first manually mapped with a hand projector to determine its location, ocular dominance, eccentricity, and approximate preferred orientation. The display screen was then centered on the neuron’s receptive field, and computer-generated stimuli were presented to the neuron’s dominant eye. Test conditions were randomly interleaved, and poststimulus time histograms (PSTHs) were collected and integrated to obtain an average spike frequency as a function of the stimulus parameter being varied. First, the neuron’s optimal grating parameters (orientation and spatial frequency) were determined. The grating’s contrast and drifting temporal frequency were 30% and 3 Hz, respectively. Abutting gratings were initially tested with the envelope orientation set to the neuron’s optimal grating orientation, and the envelope spatial frequency was set to half the optimal grating value. The envelope’s drifting temporal frequency and contrast were 3 Hz and 100%, respectively. The carrier was stationary and had a contrast of 70% (sinewave) or 100% (line). These initial settings for the envelope parameters were chosen on the basis of preliminary results, and they usually represented near-optimal values for most abutting grating responsive neurons. A series of carrier spatial frequencies were tested, ranging from a

value at or below the neuron’s grating resolution up to nearly the resolution limit of the CRT screen. In the case of abutting line gratings, the line width was kept at 10% of one carrier cycle.

As explained in the introduction, linear summation would fail to account for neuronal responses at very high carrier spatial frequencies. Accordingly, we classified responses to abutting gratings as nonlinear if two criteria were met: first, significant responses (*t*-test, compared to spontaneous activity) should be found at relatively high frequencies that were well beyond the neuron’s luminance resolution; second, these high-frequency responses should be bandpass. The subsequent series of experiments was conducted only on neurons showing such nonlinear responses. The envelope spatial frequency and orientation were then each varied independently using the neuron’s measured optimal high carrier spatial frequency. Unless noted otherwise the carrier orientation was always kept orthogonal to the envelope, which would be expected to drive strong IC responses (Kennedy, 1978; von der Heydt & Peterhans, 1989; Soriano et al., 1996; Westheimer & Li, 1996). Using optimal spatial frequencies for the envelope and the carrier, along with optimal envelope orientation, carrier orientation tuning was then measured over a 180-deg range.

Data analysis

Neurons were classified as simple or complex based on the ratio of modulated to mean responses (AC/DC) measured with optimal gratings (Skottun et al., 1991). Data were summarized in plots of average spike frequency (with spontaneous activity subtracted) as a function of the stimulus parameter being varied. Optimal parameter values were obtained from Gaussian curve fits to relevant portions of such plots.

Circular variance (CV), an index of tuning bandwidth for parameters such as orientation or phase (Marida, 1972; Ringach et al., 1997), was calculated as

$$CV = 1 - \frac{\left| \sum_k R_k \exp(i2\theta_k) \right|}{\sum_k R_k}, \quad (1)$$

where R_k was the response strength at phase or orientation θ_k . CV values range from zero (perfectly sharp tuning) to unity (isotropic response).

An index of overall motion direction selectivity (DSI) was taken as

$$DSI = (R_P - R_N)/(R_P + R_N) \times 100\%, \quad (2)$$

where R_P and R_N were neuronal responses to the preferred and nonpreferred grating directions, respectively. Thus for gratings, the DSI was always nonnegative. However, for neurons preferring the opposite direction for abutting gratings, the DSI would be negative. The absolute value of DSI typically ranged from 0% (nondirectional) to 100% (completely directional).

Results

Two kinds of abutting grating responses

Bimodal tuning to carrier spatial frequency

We tested neuronal responses to abutting gratings over a large range of carrier spatial frequencies and compared the neurons’

preferred spatial frequencies to carriers of the abutting gratings and to simple gratings. If neurons respond to low carrier spatial frequencies that overlap with the neuron's luminance passband, the responses could be explained in terms of linear summation within the conventional receptive field (Fig. 2A). In contrast, at carrier spatial frequencies much higher than the neurons' luminance passband, the light and dark regions of the stimulus will cancel out within the neurons' receptive field, and no responses would be predicted from a linear mechanism (Fig. 2C). Thus responses to a high carrier spatial frequency indicate a nonlinear mechanism.

About 40% of 136 neurons tested in this way exhibited bimodal tuning with distinct peaks at both low and high carrier spatial frequencies. Fig. 2 illustrates a typical result from one neuron (filled circles and solid line): at low carrier spatial frequencies, this neuron showed bandpass tuning to abutting gratings (0.03–0.1

cpd, with a peak response at 0.04 cpd), which was within the range of grating spatial frequency response (open circles and dashed line, 0.04–0.30 cpd). Therefore this abutting grating response might be explained at least in part by a linear mechanism responding to local luminance edges (Fig. 2A). Across a higher range of frequencies (0.13–0.60 cpd) the responses declined sharply. However, at still higher carrier spatial frequencies (0.80–3.0 cpd) the responses became vigorous again, with a second peak response at 2.2 cpd. In contrast, the neuron did not respond to simple gratings (open circles and dashed line) in a similar range of high spatial frequencies. In this second passband of abutting grating responses, the local luminance edges are well beyond the neuron's grating resolution (Fig. 2C), and therefore these responses reflect a fundamentally nonlinear mechanism. Thus the bimodal responses indicate that the same neuron can respond to abutting gratings in two

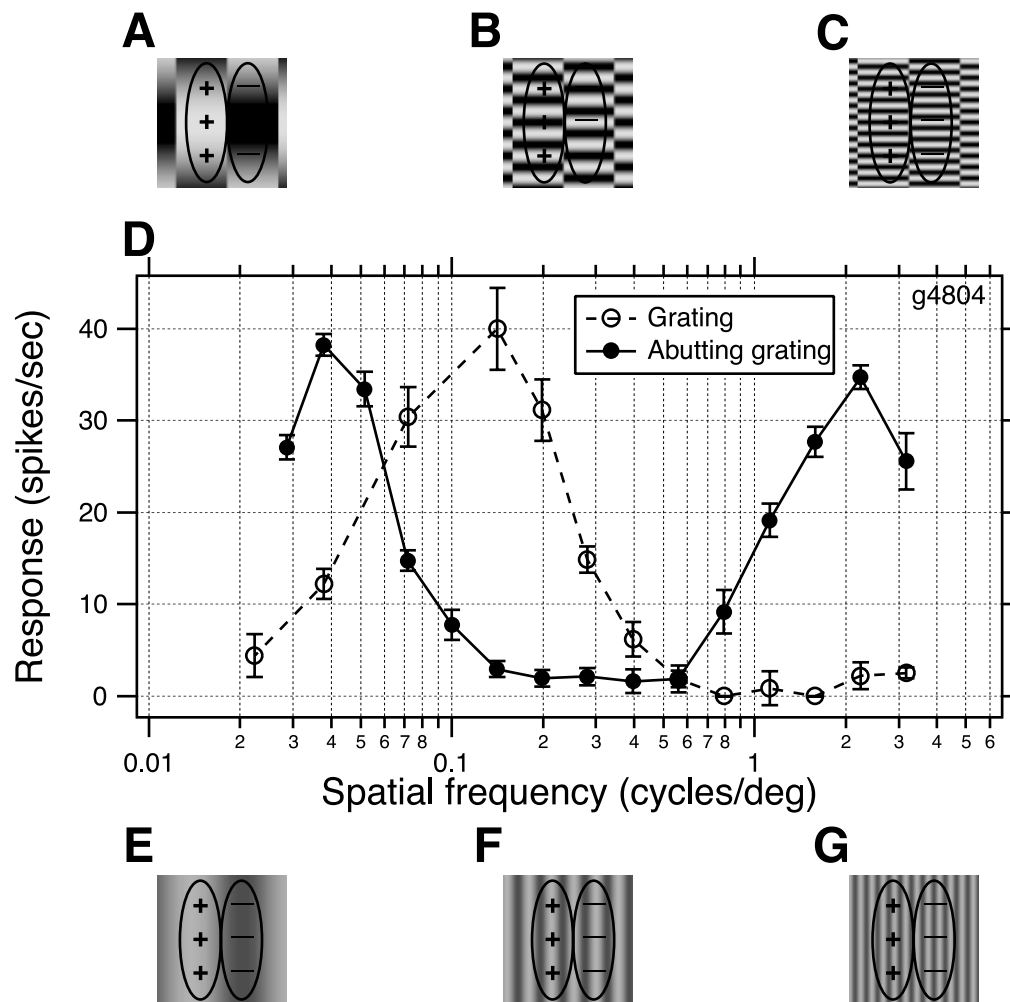


Fig. 2. A typical neuron's spatial frequency tuning to carriers of abutting sinewave gratings and to luminance gratings. Abutting sinewave gratings with carrier spatial frequencies from low to high are shown in A–C, superimposed on cartoon linear RFs with excitatory and inhibitory zones. Gratings with spatial frequencies from low to high are shown in E–G, superimposed on linear RFs. Notice that the linear RF that will respond to gratings with low spatial frequency (E) will also respond to abutting gratings with comparably low carrier spatial frequency (A) but not to those with high carrier spatial frequency (C). Neuronal responses to abutting gratings are shown as a function of carrier spatial frequency in D (solid lines and closed circles); envelope orientation, 0 deg; spatial frequency, 0.07 cpd; temporal frequency, 3 Hz; carrier orientation, 90 deg; contrast, 70%. The same neuron's response as a function of grating spatial frequency is shown in D as dashed lines and open circles; orientation, 0 deg; temporal frequency, 3 Hz; contrast, 30%. Here and in subsequent figures, spontaneous activity has been subtracted, and error bars indicate standard errors. Note that the optimal carrier spatial frequency (2.2 cpd) is much greater than the optimal grating spatial frequency (0.14 cpd).

categorically distinct ways, depending on the carrier spatial frequency—a linear luminance-driven response at low carrier spatial frequencies and a nonlinear response at high carrier spatial frequencies.

Conceivably the second passband at high carrier frequencies could be mediated by integrating inputs from a set of fine-scale linear subunits, oriented either parallel or orthogonal to the carrier. While such a model seems rather unlikely, a testable prediction would be that such a neuron should respond to a high spatial frequency grating that is oriented either parallel or orthogonal to the carrier. We have already seen that the neuron in Fig. 2 did not respond to gratings that were oriented orthogonal to the carrier in the high spatial frequency range (open circles and dashed line, 0.80–3.0 cpd). Two more examples of such control experiments are shown in Fig. 3. When tested with abutting gratings at the optimal grating orientation (filled circles and solid line), the neuron in Fig. 3B responded at two distinct carrier spatial frequency ranges. In contrast, the neuron showed no significant responses to gratings in the range of the high spatial frequency carrier response (0.5–2.0 cpd), whether the grating was oriented orthogonal (open circles and dashed line) or parallel (open squares and dotted line) to the carrier. Another example (Fig. 3C) showed a smaller but significant response to abutting gratings at high carrier spatial frequencies (1.0–2.0 cpd), while responses to gratings over the same spatial frequency range were negligible, irrespective of orientation. Therefore the abutting grating responses at high carrier spatial frequencies cannot be ascribed to fine-scale linear subunits. Since it is well known that orientation selective neurons only have a single, limited range of preferred grating spatial frequencies (as further confirmed by our control experiments), in the following experiments we only measured grating responses over low spatial frequencies to capture the classical (luminance) spatial tuning curve.

Fig. 4 shows additional examples of neurons' carrier spatial frequency responses to abutting sinewave gratings to illustrate the range of results. The left-hand panels show data from three neurons exhibiting bimodal responses. These neurons' preferred high carrier spatial frequencies (>0.4 cpd) did not overlap with the lower frequency grating passbands in all cases, and the response magnitudes were less than (Fig. 4B) or about equal to (Figs. 4A & C) peak grating responses. The low carrier spatial frequency peak (<0.06 cpd) ranged from being similar to the neuron's preferred grating spatial frequency (Fig. 4A) to about 1–2 octaves lower (Figs. 4B & 4C). Some neurons only responded unimodally to abutting gratings with relatively low carrier spatial frequencies, which overlapped with the neurons' luminance passbands—three examples are shown in Figs. 4D, E, and F.

In all examples we have shown, the relationship between these low carrier frequency peaks and the optimal grating responses varied from one neuron to another in both relative amplitudes and spatial frequencies. This varying relationship could plausibly be due to differing aspect ratios (length *vs.* width) of linear RFs and to the relative alignments of the carrier phase with the RFs, which were not parametrically optimized in these measurements. A neuron's optimal grating spatial frequency is related to the width of the RF (Fig. 2E), but the neuron's preferred low carrier spatial frequency is related to the length of the RF (Fig. 2A). Thus, the low carrier frequency peak would be similar to the grating frequency peak (Fig. 3B; Figs. 4A & E) when neurons' RF aspect ratios are about 1:1. When the aspect ratios are larger or smaller than 1:1, the low carrier frequency peak would be lower (Fig. 2D; Fig. 3C;

Figs. 4B, C, & D) or higher (Fig. 4F) than the grating frequency peak, respectively. Few cells appeared to have an aspect ratio smaller than 1:1, which is consistent with previous studies (Jones & Palmer, 1987; Pei et al., 1994). Another factor that may influence the neuron's preferred low carrier frequency is carrier phase, whose influence will be discussed below (Figs. 6 & 7).

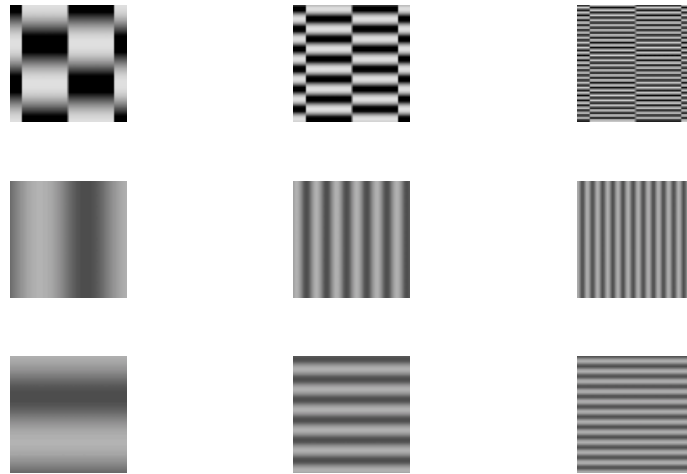
Altogether about 40% of the neurons in our sample (55/136) showed bimodal tuning (Figs. 4A–C) and 30% (40/136) only showed significant responses at low carrier spatial frequencies (Figs. 4D–F). Another 23% (31/136) responded only to high frequencies, even though in theory all neurons responding to luminance gratings should respond to abutting gratings at low enough carrier spatial frequencies. It is possible that in some cases the tested range of frequencies was not sufficiently low, or more likely the fixed value of carrier phase (0 deg) used in these experiments might have been fortuitously inappropriate for some neurons' RFs. Carrier phase sensitivity will be explored in the following section. The remaining 7% of the sampled neurons either showed a very broadband response without two distinct peaks or failed to respond to abutting gratings in the tested range. The subsequent analysis only included the 63% (86/136) of neurons that showed either bimodal tuning or responses only to high carrier frequencies.

We also investigated whether abutting line gratings could evoke linear and nonlinear responses in the same neurons that showed bimodal tuning to abutting sinewave gratings. The carrier spatial frequency of abutting line gratings was varied across a similar range as abutting sinewave gratings, and the line width was kept at 10% of the carrier spatial period. All the sampled neurons demonstrated a similar bimodal tuning to the carrier spatial frequency of abutting line gratings—three examples are shown in Fig. 5. One neuron (Fig. 5A) responded when the carrier spatial frequencies of abutting line gratings were ~ 0.02 – 0.07 cpd (open squares and solid line), within the neuron's luminance passband (0.02–0.07 cpd, open circles and dashed line). This neuron's responses dropped quickly at higher carrier frequencies but increased again in the range of 0.3–3.0 cpd, which was outside of the neuron's luminance passband. The same neuron shows a similar bimodal response to abutting sinewave gratings (filled circles and solid line). Two other neurons (Figs. 5B & C) also exhibited similar bimodal tuning to carrier spatial frequency for both abutting line and sinewave gratings.

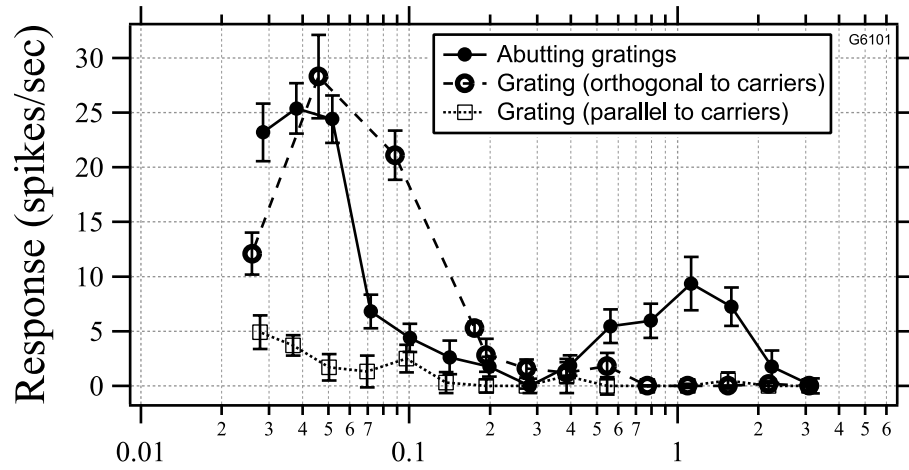
In the high-frequency range, the abutting lines produced a broader bandwidth and a lower peak value than abutting sinewave gratings. The broader bandwidth to abutting lines might be due to the broader band of spatial frequencies they contain since they are hard-edged. Since the lines are wider at lower spatial frequencies, their luminance contrast is comparable to that of abutting sinewave gratings of a higher frequency, which might explain the misalignment of high-frequency peaks. Despite the small differences in the frequency peak, the effective low and high bands of carrier spatial frequencies for both stimuli were substantially overlapping, which held for all of the 15 neurons tested.

Thus neuronal responses to abutting gratings (both sinewave and line types) can be mediated by distinct linear and nonlinear mechanisms depending on the carrier spatial scale relative to the neuron's grating preferences. At low spatial frequencies where local luminance contrast is resolvable by the neuron's classical RF, the neuron would respond to the luminance edges through a linear mechanism. On the other hand, responses observed at very high spatial frequencies, beyond the neuron's luminance resolution, must be mediated by a spatially nonlinear mechanism.

A



B



C

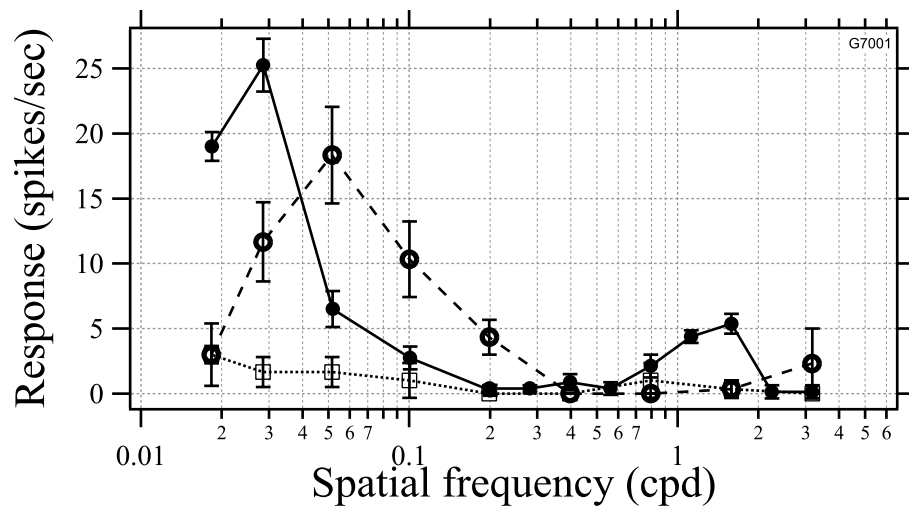


Fig. 3. Control experiments in which neuronal responses to carrier spatial frequency are compared with those to grating spatial frequency over the same range. A, examples of abutting gratings with carrier spatial frequencies from low to high, are shown in the first row, from left to right. Examples of gratings oriented orthogonal to the carriers, whose spatial frequencies vary from low to high are shown in the second row, from left to right. Examples of gratings oriented parallel to the carriers are similarly shown in the third row, from left to right. B and C, respectively: neuronal responses are plotted against carrier spatial frequency of abutting gratings (filled circles and solid lines), gratings oriented orthogonally (open circles and dashed lines), or parallel (open squares and dotted lines) to the carriers. Other parameters used for B and C, gratings: orientation, 150 deg, 120 deg (open circles and dashed lines) and 60 deg, 30 deg (open squares and dotted lines); temporal frequency, 3 Hz; contrast, 30%. Abutting gratings: envelope orientation, 150 deg, 120 deg; envelope spatial frequency, 0.03 cpd, 0.05 cpd; temporal frequency, 3 Hz; carrier orientation, 60 deg, 30 deg; contrast, 70%. Notice that both neurons responded to abutting gratings at high carrier spatial frequencies but not to gratings over the same frequency range regardless of their orientation.

Carrier phase dependence

In the previous section, we speculated that the carrier phase (relative to the neuron's RF) might influence linear responses, resulting in variations in both relative amplitudes and spatial frequencies of the low carrier frequency peaks and the optimal grating frequency peaks. More generally, spatial phase dependence is a signature of linear spatial summation, while phase invariance is an indication of nonlinear processing (Spitzer & Hochstein, 1985a,b).

For simple cells, which have spatially discrete subregions, linear responses to abutting gratings would be strongest when the carrier phase is optimally aligned with a neuron's RF (Fig. 6A) and much weaker or even absent at a misaligned carrier phase (Fig. 6B). In contrast, responses at a high carrier spatial frequency would hardly be affected by carrier phase since they are generated by a nonlinear mechanism (Grosf et al., 1993). Although complex cells do not have clearly distinct subregions (but see Spitzer &

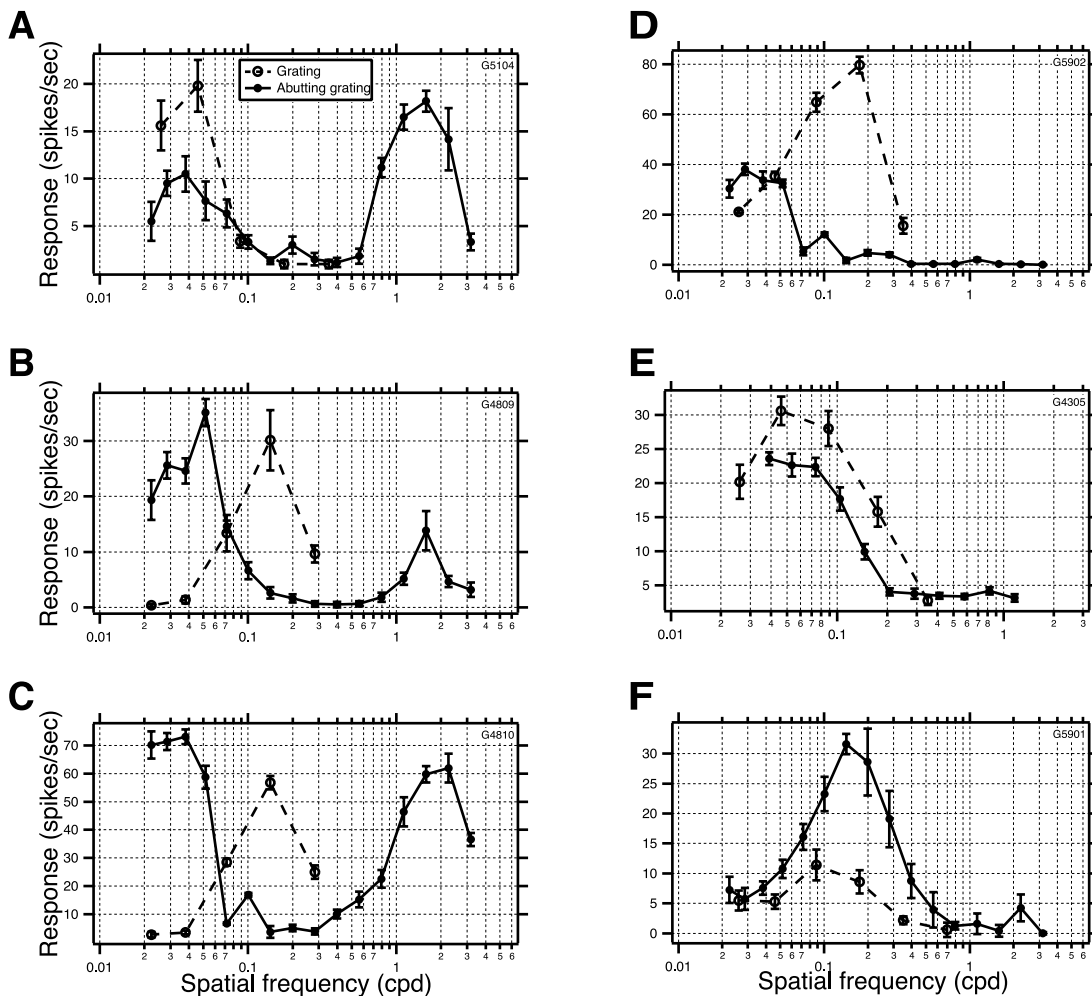


Fig. 4. Six neurons' spatial frequency tuning for abutting grating carriers and for gratings, in same format as Fig. 2. A, B, C, three neurons that showed bimodal tuning to carrier spatial frequency. D, E, F, three neurons that responded only at low carrier spatial frequencies. Envelope spatial frequency for A-F, respectively: 0.03, 0.09, 0.07, 0.03, 0.07, and 0.05 cpd.

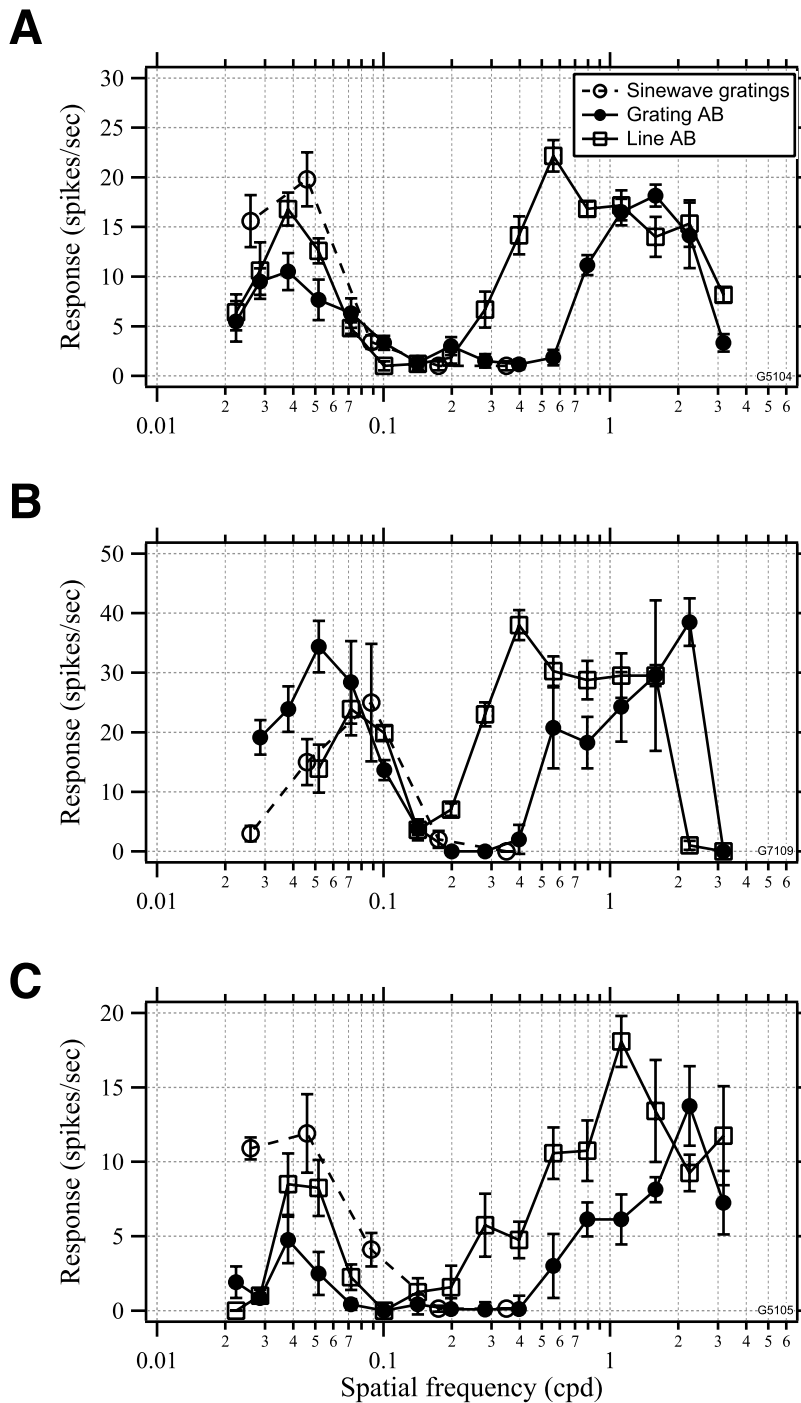


Fig. 5. Three neurons' responses to carrier spatial frequency of abutting gratings (both line and sinewave types). Neuronal responses are plotted against carrier spatial frequency of abutting line gratings (open squares and solid lines), abutting sinewave gratings (filled circles and solid lines), and spatial frequency of gratings (open circles and dashed lines). A–C, gratings: orientation, 0 deg, 90 deg, 0 deg; temporal frequency, 3 Hz; contrast, 30%. Abutting sinewave and line gratings: envelope orientation, 0 deg, 90 deg, 0 deg; envelope spatial frequency, 0.3 cpd, 0.5 cpd, 0.3 cpd; temporal frequency, 3 Hz; carrier orientation, 90 deg, 0 deg, 90 deg; contrast, 70%. For abutting line gratings, the line width was kept at 10% of a carrier spatial cycle.

Hochstein, 1985b), it is reasonable to suppose that they sum rectified subunits that are spatially linear in a similar way (Hubel & Wiesel, 1962). Thus the carrier phase-dependence of complex cells' abutting grating responses might also indicate whether or not the underlying mechanism is linear.

We investigated how carrier phase influenced abutting grating responses of bimodal neurons at their optimal low and high carrier spatial frequencies. Fig. 6 displays polar plots of typical carrier phase responses for a simple cell (Figs. 6C & D) and a complex cell (Figs. 6E & F). When tested at the low optimal carrier spatial

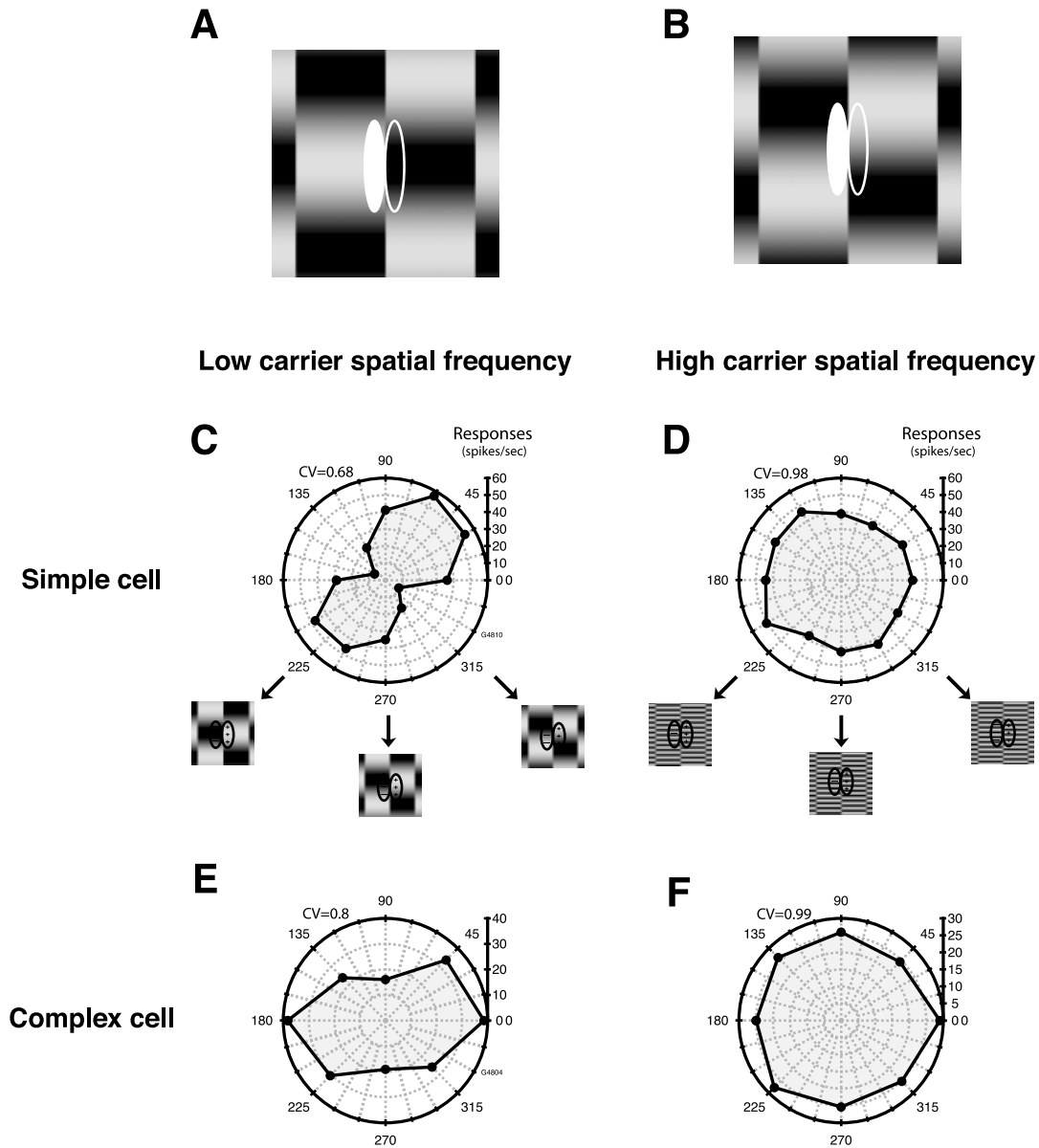


Fig. 6. Dependence on carrier phase. A simple cell's RF is shown superimposed on abutting gratings with relatively low carrier spatial frequency, either aligned (A) or misaligned (B) with the carrier phase. C–F show two neurons' responses to carrier phase at their optimal low and high carrier spatial frequencies. Distance from the origin represents response strength (spikes/s); angular subtense represents carrier phase (0 deg–360 deg). A simple cell's carrier phase responses are shown when the carrier spatial frequency was optimally low (C) or high (D). A complex cell's carrier phase responses are shown when the carrier spatial frequency was optimally low (E) or high (F). CV, indicating the degree of carrier phase dependence, is shown on the upper left corner of each plot. Examples of stimuli used are shown below the polar plots of C and D, superimposed with a spatially linear RF. Stimulus parameters for C–F, respectively: envelope orientation, 30 deg, 30 deg, 60 deg, 60 deg; envelope spatial frequency, 0.07 cpd; carrier orientation, 120 deg, 120 deg, 150 deg, 150 deg; carrier spatial frequency, 0.05 cpd, 2.2 cpd, 0.04 cpd, 2.5 cpd. For both cells, responses were clearly phase-dependent at the low carrier spatial frequency but phase-invariant at the high frequency.

frequency (Figs. 6C & E), both cells showed phase-dependent responses. Notice that the difference between preferred and non-preferred carrier phase is 90 deg for both cells, corresponding to the maximum difference in stimulus alignment with a cell's RF. In contrast, when tested at the high optimal carrier spatial frequency, both neurons showed relatively uniform responses across all the carrier phases (Figs. 6D & F). Thus for both simple and complex cells, abutting grating responses at low carrier frequency were

sensitive to the carrier phase, while high-frequency responses were invariant, suggesting that carrier phase dependence might provide an additional signature of linear *vs.* nonlinear responses.

Fig. 7 illustrates the relationship between carrier phase dependence, response type (low or high optimal carrier spatial frequency), and cell type (simple or complex) for 12 neurons that showed bimodal responses. The abscissa shows the degree of phase dependence as measured by CV (eq. (1)), which ranges from

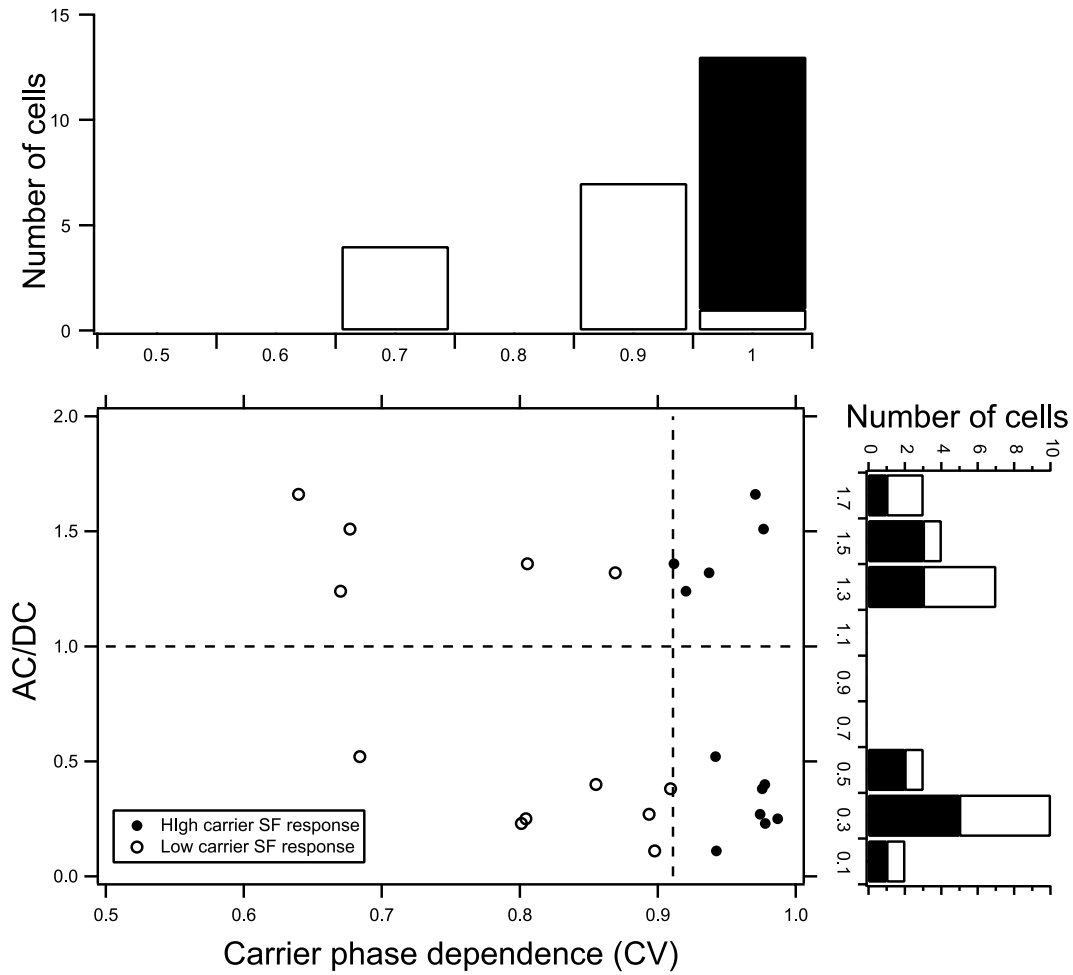


Fig. 7. Scatter plot showing relationship between cell type (simple vs. complex) and carrier phase dependence, for responses obtained at optimally low (open circles) or high (filled circles) carrier spatial frequencies. Ordinate indicates response modulation (AC/DC ratio, >1 for simple and <1 for complex cells); abscissa shows carrier phase dependence (CV). The histogram on the right shows a bimodal distribution of AC/DC ratios, corresponding to simple vs. complex type cells. The histogram on the top plots number of cells against CV. Note that responses at low carrier spatial frequencies are more carrier phase-dependent (CV < 0.9), while responses at high frequencies are relatively phase-invariant (CV > 0.9), for both simple and complex type cells.

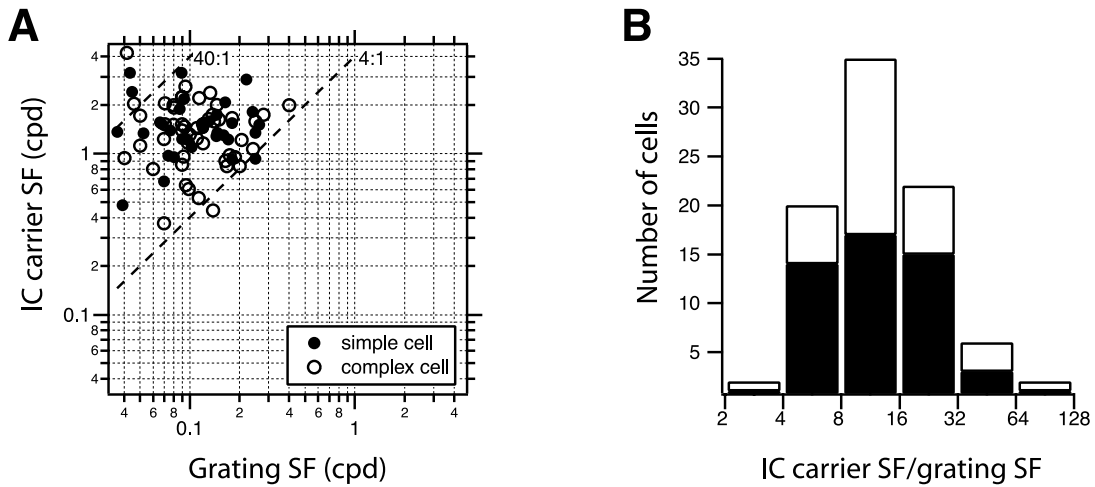


Fig. 8. Relationship between optimal spatial frequencies of gratings and IC carriers for 86 neurons. A, scatter plot of optimal IC carrier spatial frequencies against optimal grating spatial frequencies, for simple cells (filled circles) and complex cells (open circles). B, distribution of neurons' optimal spatial frequency (SF) ratio (carrier/grating). Black bars represent simple cells ($N = 35$), and solid bars represent complex cells ($N = 51$).

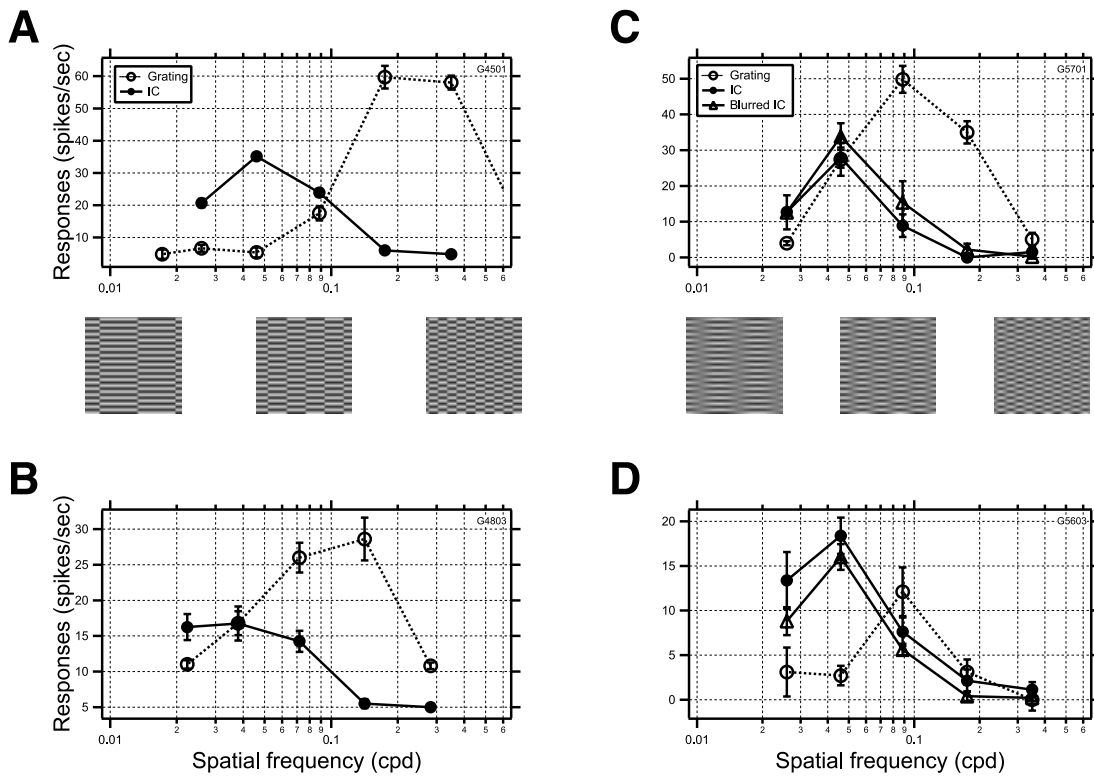


Fig. 9. Four neurons' spatial frequency tuning to IC envelopes and to gratings. Neuronal responses (spikes/s) are plotted against IC envelope spatial frequency of either abrupt (IC, solid lines and closed circles) or sinusoidal (blurred IC, solid lines and open triangles) phase changes. Grating spatial frequency responses are also shown (dashed lines and open circles). Examples of ICs and blurred ICs with different envelope spatial frequencies are shown below A and B, respectively. Carrier spatial frequencies for A–D: 1.6 cpd, 1.5 cpd, 1.0 cpd, 1.6 cpd.

zero (response at only one phase) to unity (ideal phase invariance). The degree to which grating responses are modulated (simple vs. complex behavior) is measured as the AC/DC ratio (Skottun et al., 1991), shown on the ordinate. Responses obtained at optimally low and high carrier spatial frequencies are represented with open or filled circles. The AC/DC ratios were bimodally distributed (histogram at right), consistent with previous studies (Skottun et al., 1991). The carrier phase dependence for simple cells was not significantly different from that for complex cells (two-tailed *t*-test, $P > 0.05$). However cells were clearly divided into two groups based on the CV values (Fig. 7, scatter plot and histogram at the top): high carrier spatial frequency responses (filled circles) have larger CVs, indicating that responses are uniform across carrier phase, while low frequency responses (open circles) have smaller CVs, showing carrier phase dependence. Although the dividing line (CV = 0.9) is drawn subjectively from the data, without exception each neuron had a higher CV for high than for low carrier spatial frequency responses (paired two-tailed *t*-test, $P < 0.02$).

Thus carrier phase sensitivity provides additional reinforcing evidence for two kinds of abutting grating processing: at the optimal high carrier spatial frequency, a phase-invariant (nonlinear) mechanism, and at the optimal low frequency, a phase-dependent (linear) mechanism.

Mechanism of IC responses

We have demonstrated that nonlinear responses to abutting gratings (IC responses) occurred when the carrier spatial frequency of

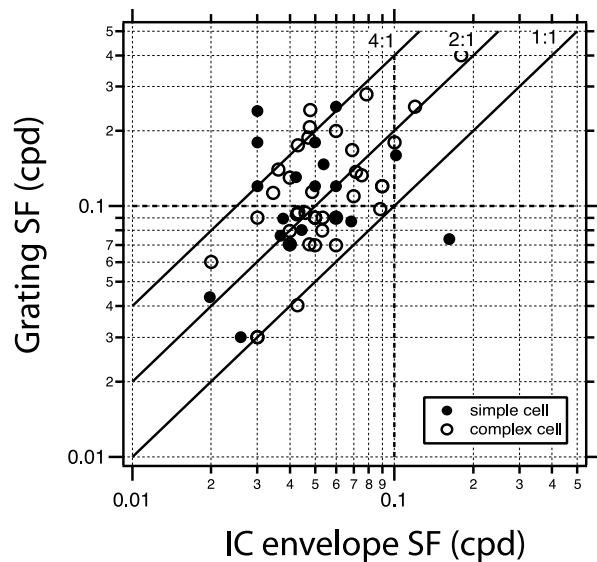


Fig. 10. Scatter plot showing relationship between optimal spatial frequencies of gratings and IC envelopes for 57 neurons. Filled circles represent simple cells ($N = 19$), and open circles represent complex cells ($N = 38$). Notice that most neurons preferred a lower spatial frequency for IC envelopes than for the gratings (median ratio = 0.4; $N = 57$ cells). The distribution of optimal grating spatial frequencies was centered around the line of 0.1 cpd, ranging from 0.03 to 0.4 cpd; in contrast, neurons' optimal IC envelope spatial frequencies were usually lower than 0.1 cpd with only 5 exceptions.

the stimulus was well beyond the neuron's luminance passband. By using appropriate stimuli, we next quantitatively explored the physiological properties of IC processing. Since we have demonstrated that abutting line and sinewave grating components are equally effective in driving the IC response (Fig. 5), we subsequently only use sinewave grating components since the parameters are mathematically well defined and bimodal neurons demonstrated more clearly separate low and high carrier spatial frequency response ranges.

Carrier spatial frequency tuning

As demonstrated earlier, a given neuron's optimal carrier spatial frequency for ICs is much higher than its preferred grating spatial frequency (Figs. 2, 3, & 4). To examine whether there is a fixed relationship between these two parameters, we measured both the optimal carrier and grating spatial frequencies for 86 neurons. Nearly all neurons' optimal carrier spatial frequencies were at least four times higher than their optimal grating frequencies (Fig. 8A). Although individual neurons showed different ratios of optimal carrier to grating spatial frequency, 88% exhibited a ratio in the range of 4 to 32 (Fig. 8B, median ratio = 12.7).

Dependence on envelope spatial frequency

We examined neurons' envelope spatial frequency dependence, fixing the carrier spatial frequency at optimal values. Fig. 9 depicts typical examples in which the envelope (solid line, filled circles) and luminance (dashed lines, open circles) spatial frequency responses are compared for each cell. Fig. 9A shows a complex cell that was bandpass tuned to the IC envelope spatial frequency, with a peak response at ~ 0.05 cpd (filled circles) that was about five times lower than its preferred grating frequency (~ 0.2 – 0.4 cpd, open circles). Another complex cell (Fig. 9B) showed a low-pass response to envelope spatial frequency over the tested range: this neuron responded only at IC envelope spatial frequencies lower than its optimal grating frequency (~ 1 – 2 cpd). Another two neurons, complex and simple, respectively (Figs. 9C & D), were bandpass tuned to both kinds of spatial frequency, with peaks about an octave apart.

Conceivably the difference in modulation profiles (sinusoidal for gratings vs. abrupt squarewave-like for ICs) could contribute to the different spatial scale preferences for the two stimuli. If so, ICs with a "blurred" envelope (having sinusoidal phase transitions; see stimulus images below Fig. 9C) might evoke responses over a slightly different range than stimuli without abrupt phase shifts,

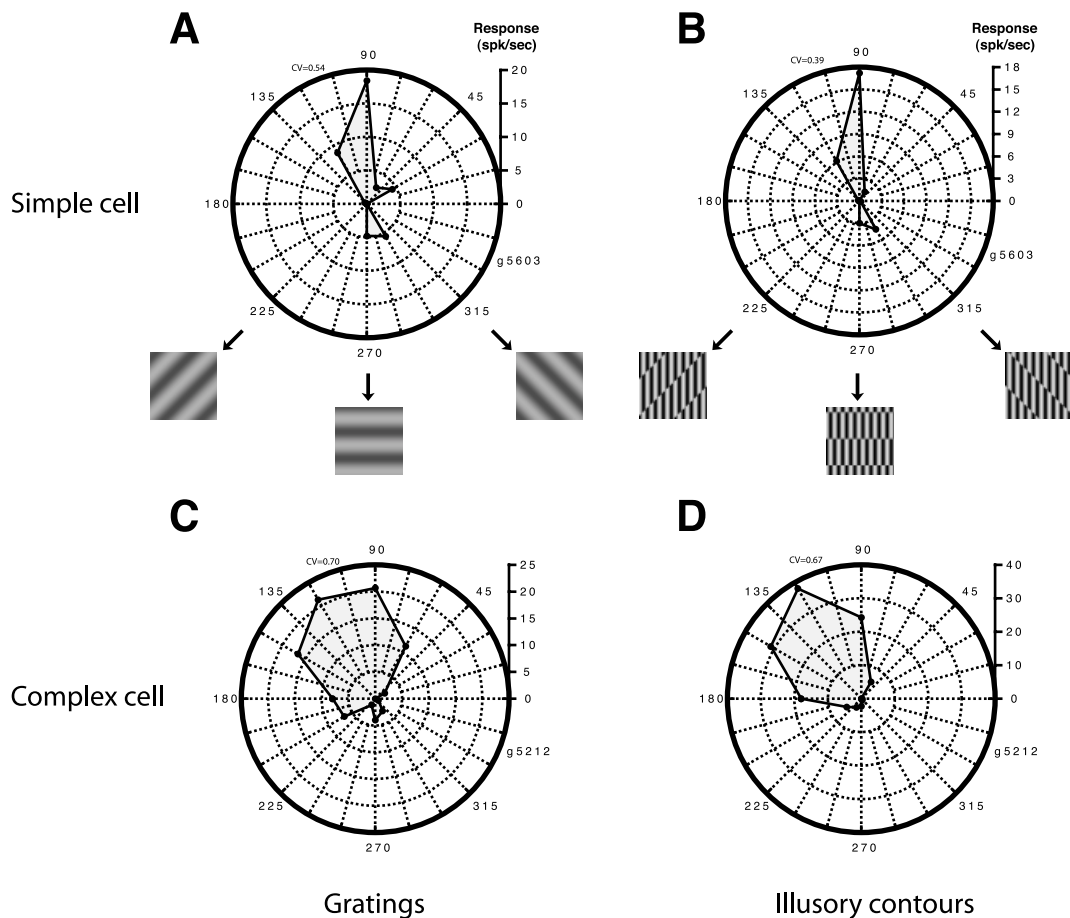


Fig. 11. Polar plots of orientation tuning to luminance gratings (A and C) and ICs (B and D), for two neurons, in the same format as Fig. 6. Snapshots of representative stimuli with different orientations are shown below A (gratings) and B (ICs). A and B are measurements from a simple cell, C and D from a complex cell. Grating spatial frequencies for A and C: 0.09 cpd; envelope spatial frequencies for B and D: 0.05 cpd; carrier spatial frequency for B and D: 1.6 cpd.

since the latter contain broader spatial components in the Fourier domain. However, the envelope spatial frequency tuning for normal vs. blurred ICs was similar for all 10 neurons tested—two typical examples are shown in Figs. 9C and D, both of which displayed similar envelope spatial frequency tuning for both normal (filled circles, solid lines) and blurred (open triangles, solid lines) ICs. Thus the different spatial preferences for gratings and ICs are more likely due to the different processing of luminance vs. nonluminance stimuli, rather than to the presence or absence of local edge features.

Fig. 10 displays the relationship between neurons' optimal grating spatial frequency and the same neurons' optimal IC envelope spatial frequency for 57 neurons (38 complex and 19 simple cells). Optimal envelope spatial frequencies were usually lower than 0.1 cpd with only four exceptions. In contrast, these neurons' optimal grating spatial frequencies were equally distributed about 0.1 cpd, ranging from 0.03 to 0.4 cpd, consistent with previous reports for A18 neurons (Movshon et al., 1978; Ferster & Jagadeesh, 1991). A majority of neurons (86%, 49/57) had ratios of optimal grating to envelope spatial frequencies ranging from 1:1 to 4:1 (median ratio ~ 2.5).

Selectivity for envelope orientation and direction of movement

Although neurons had different spatial frequency preferences for luminance gratings and ICs, their preferred orientations for the two kinds of stimuli were similar (Fig. 11). For example one simple cell (Figs. 11A & B) showed quite similar optimal orientation and bandwidth for the two stimuli. Figs. 11C & D show analogous results from a complex cell with similar, though broader, orientation tuning to both gratings and ICs.

Fig. 12A depicts 37 neurons' optimal grating orientations plotted against their optimal IC envelope orientations (23 complex and 14 simple cells). Most data points, for both simple and complex cells, clustered around a unity ratio (mean grating/envelope orientation = 0.99), demonstrating similar orientation preferences for both stimuli. Fig. 12B compares the orientation tuning bandwidth (CV) for gratings (ordinate) and ICs (abscissa) for the same neurons. Somewhat more than half the cells (70%, both complex and simple types) had orientation tunings for IC envelopes that were broader than for gratings, and the bandwidths for the two stimuli were moderately correlated ($r = 0.61$).

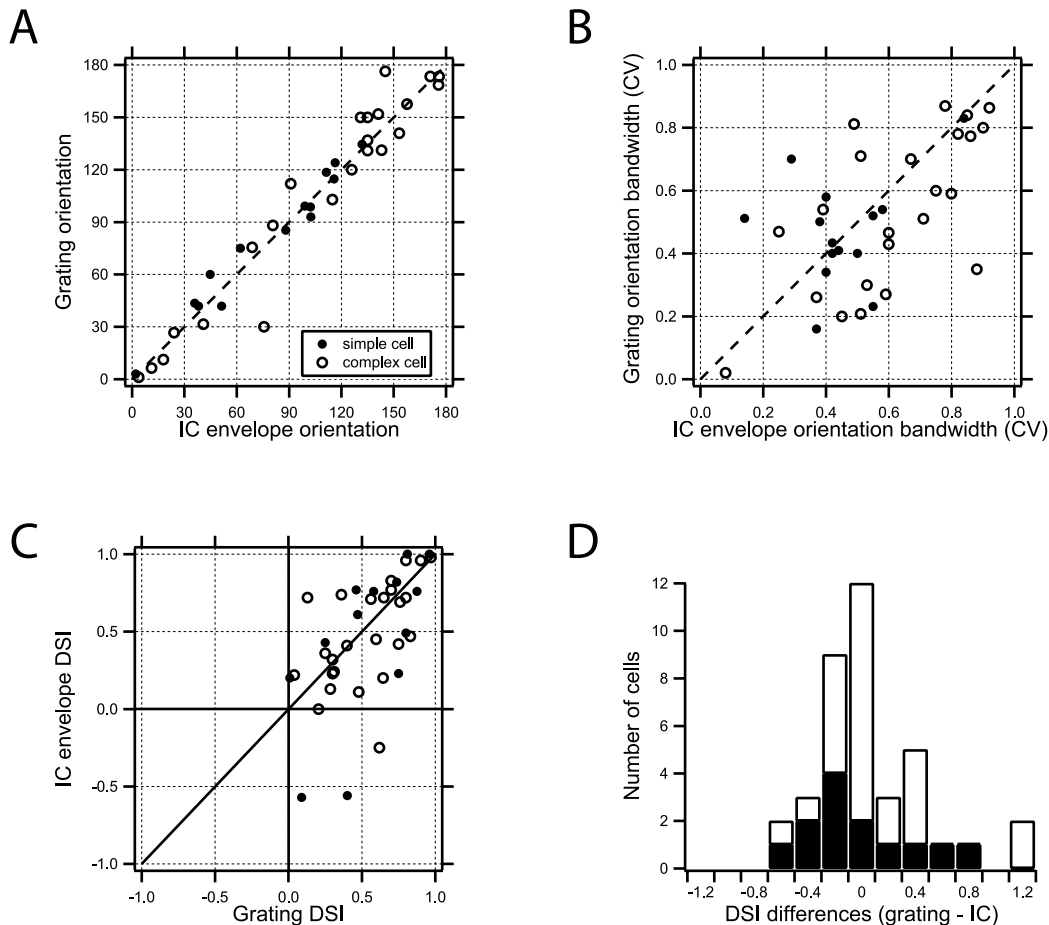


Fig. 12. Orientation and direction tuning to IC envelopes vs. gratings for 14 simple cells (filled circles) and 23 complex cells (open circles). A, scatter plot showing the same neurons' optimal orientations for IC envelopes vs. gratings. The dashed line represents equality. B, scatter plot depicting the same neurons' orientation tuning bandwidth (CV) for the two stimuli. The bandwidths for the two stimuli are moderately correlated ($r = 0.61$). C, scatter plot of direction selectivity index (DSI = $(P - N)/(P + N) \times 100\%$) for gratings vs. abutting gratings envelopes. D, distribution of DSI differences (grating DSI - IC DSI).

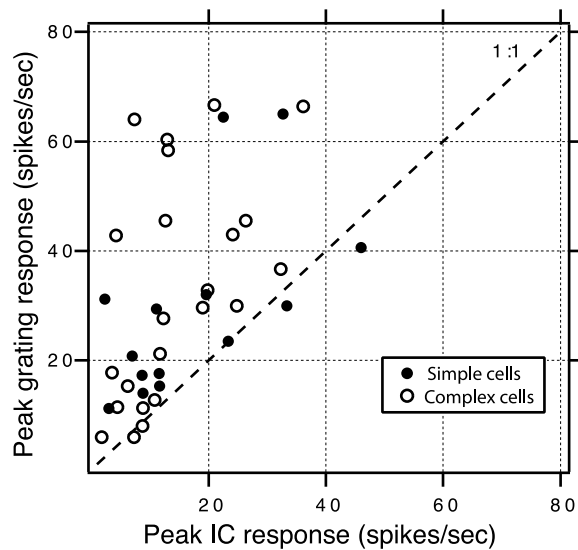


Fig. 13. Comparison of peak response amplitudes to gratings and to ICs, measured from orientation tuning data. Maximum responses (spikes/s) to grating are plotted against maximum responses to ICs, for 14 simple cells (filled circles) and 23 complex cells (open circles). On average, neurons responded around half as strongly to ICs as to gratings (mean grating/ICs = 0.55), and more than a quarter of the neurons gave IC responses that were at least 75% of their grating responses.

The two neurons in Fig. 11 had similar direction selectivity. To examine this relationship across the sampled neurons we plotted their DSIs (eq. (2)) for gratings against their DSIs for ICs in Fig. 12C. Each neuron's preferred direction was taken from its grating responses. Although individual neurons often had quite different magnitudes of directionality for gratings and ICs, 34 out of 37 had consistent preferred directions of motion. The remaining 3 neurons showed negative DSI values for ICs, indicating opposite direction preferences from gratings. The DSI differences for the two stimuli are also plotted as a histogram in Fig. 12D, showing that the differences cluster around zero (mean = 0.02).

Comparison of response strength to ICs and to gratings

Although most neurons exhibited consistent orientation and direction preferences to the two kinds of stimuli, their response strengths were often different. Fig. 13 plots the maximum responses to gratings against those to ICs for 37 neurons (from orientation tuning data like those in Fig. 11). The optimal IC responses were usually less than the same neuron's optimal luminance grating response, with a wide scatter of the relative strength among cells (from $\sim 1:1$ to $<1:4$). Neurons responded on average around half as much to ICs as to gratings (mean grating/abutting

grating response = 0.55), which accords with previous reports (von der Heydt & Peterhans, 1989). However some neurons responded quite well to ICs: more than a quarter of the neurons gave IC responses that were at least 75% of their grating responses. Response strength ratios (gratings/ICs) of simple cells were not significantly different from those of complex cells (two-tailed *t*-test, $P > 0.05$).

Dependence on carrier orientation

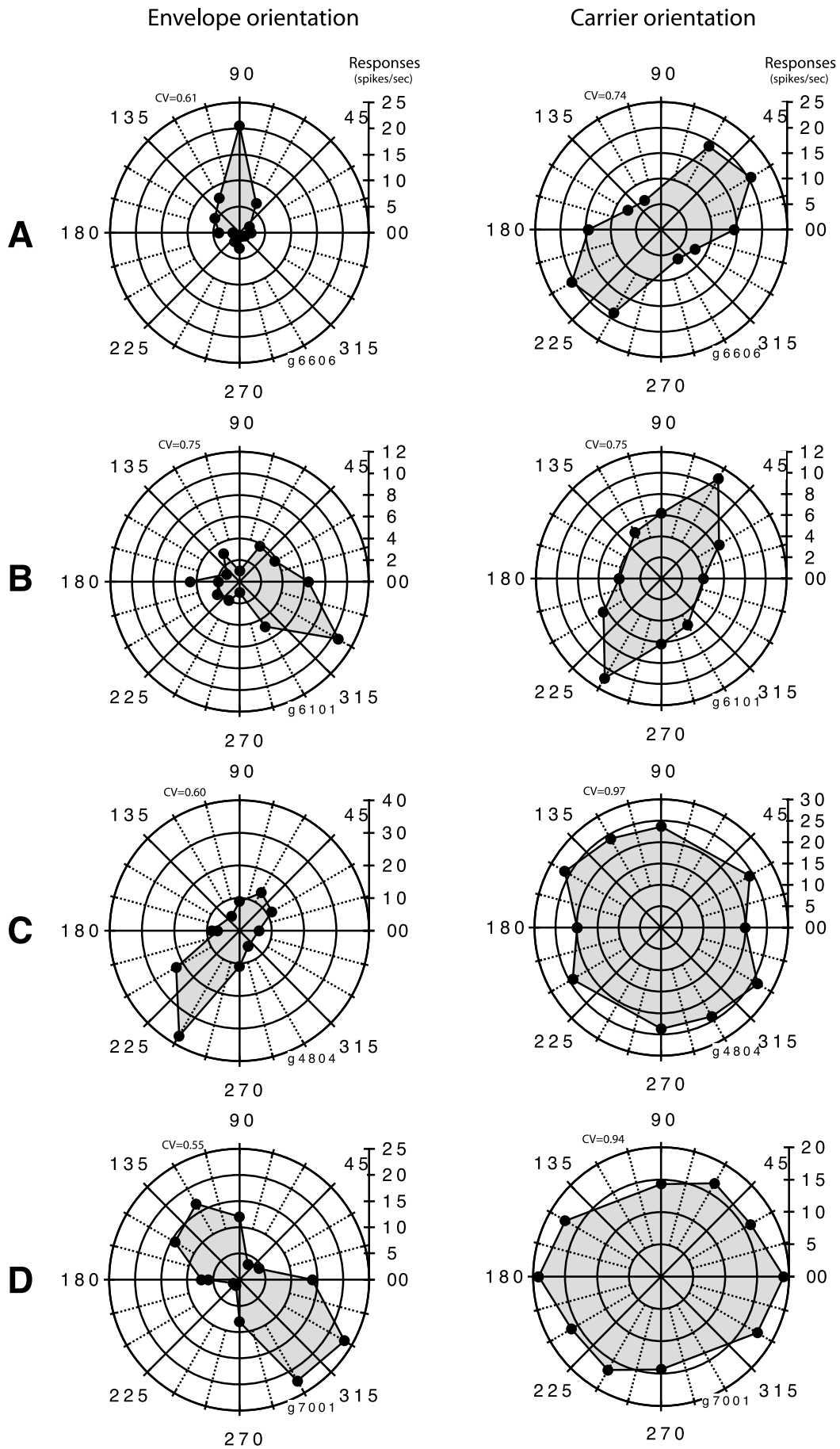
We have so far shown that neurons' responses to ICs depended on the spatial frequencies of the carrier and envelope as well as the envelope orientation. The neuron in Fig. 14A responded to a specific range of carrier orientations (right column), from 0 deg to 60 deg (and 180 deg to 240 deg), with a CV of 0.74. It was narrowly tuned for envelope orientation (left column, CV = 0.61), peaking at 90 deg, about 60 deg different from its carrier optimum. Another neuron (Fig. 14B) was also narrowly tuned for both kinds of orientation, but its optimal carrier orientation (60 deg) was orthogonal to its preferred envelope orientation (330 deg). Two other neurons (Figs. 14C & D) were broadly tuned to carrier orientation but narrowly tuned to envelope orientation. Overall, we found that orientation tuning to carriers was relatively broad, with 93% of the neurons having a CV larger than 0.7 (mean CV = 0.85, ranging from 0.43 to 0.98, for 15 simple and complex cells). Carrier CVs for simple cells did not differ significantly from those for complex cells (*t*-test, $P > 0.05$). Furthermore, we did not find any systematic relationship between a neuron's preferred envelope and carrier orientations.

To check if we have effectively driven neurons' responses by using carriers oriented orthogonal to envelopes, we compared 32 neurons' response strengths to ICs at two different carrier orientations: one orthogonal to the envelope (as in our previous protocol) and the other optimized for each neuron (Fig. 15). More than 81% of the neurons (15 simple and 17 complex cells) gave IC responses at orthogonal carrier orientations that were at least 70% of those at their optimal carrier orientations. Response strength ratios (orthogonal/optimal carriers) were on average 0.84, and the ratios for simple cells were not significantly different from those for complex cells (two-tailed *t*-test, $P > 0.05$).

Discussion

This study has demonstrated that neuronal processing of abutting gratings (either sinewave or line type) can be linear or nonlinear, depending on the spatial frequency of the carrier relative to the neuron's luminance passband. About half of A18 neurons, including both simple and complex types, exhibited both kinds of responses to abutting gratings. Further examination of the nonlinear response properties has shown two kinds of spatial frequency and orientation tuning, which is consistent with an FRF model.

Fig. 14. Neuronal tuning to carrier and envelope orientations of ICs. Distance from origin represents response strength (spikes/s), and the angular value represents orientation. We also tested neuronal responses to different IC carrier orientations over a 180-deg range, which was reflected about the origin in the polar plot, since the carriers were kept stationary. CV, an index of orientation bandwidth, is indicated at the upper left of each plot. The four neurons' envelope orientation responses are shown on the left columns, and the same neurons' carrier orientation responses are shown on the right. Neurons showed either narrow (A & B) or broad (C & D) carrier orientation tuning.



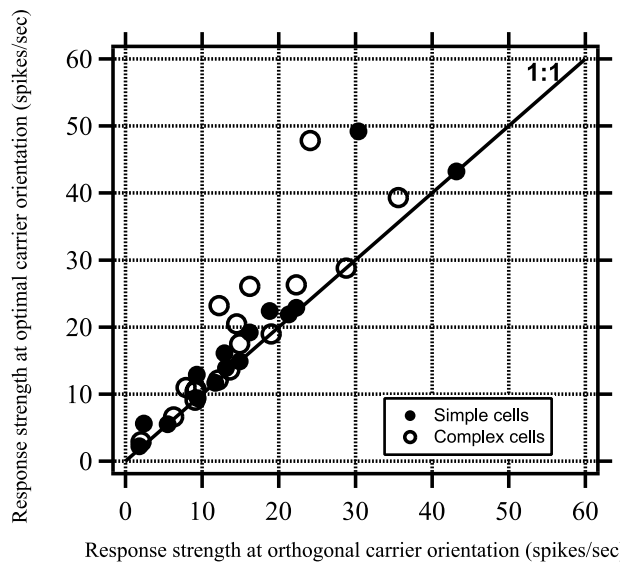


Fig. 15. Response amplitudes to ICs at carrier orientations that are either orthogonal to the envelope (as in our previous protocol) or optimized for each neuron. The neurons' response strength at preferred carrier orientation is plotted against that at carrier orientation orthogonal to the envelopes ($N = 32$, 15 simple and 17 complex cells). Most of the neurons responded almost as strongly at the two carrier orientations.

Linear and nonlinear processing of abutting gratings

We have demonstrated that nonlinear responses to abutting gratings have several properties that distinguish them from linear responses. Carrier spatial frequency plays a crucial role in differentiating linear and nonlinear responses to abutting sinewave gratings. Linear responses could be evoked by carrier spatial frequencies that overlap with the neurons' luminance passband. In contrast, nonlinear responses could be evoked when the carrier spatial frequency is within a narrow band beyond the neuron's luminance resolution. Although this band of spatial frequencies is specific for individual neurons, the ratio of optimal carrier SF/grating SF was at least four in most A18 neurons (Fig. 8).

These neurons' carrier spatial frequency tuning to abutting line gratings exhibited narrowband tuning at high frequencies similar to that for sinewave grating components (Fig. 5). In these experiments, we kept the line width at 10% of one carrier cycle in order to preserve mean luminance and net root-mean-square contrast. Thus in our experiments the greater line widths at lower carrier spatial frequencies could produce sufficient local luminance contrast to drive neural responses (left lobe of bimodal responses in Fig. 5). If we had instead kept line widths fixed at some very small value, this luminance response at low carrier spatial frequencies would probably have been attenuated or abolished. However, abutting gratings constructed from very thin lines might sometimes activate both nonlinear and linear responses. von der Heydt and Peterhans described neurons that responded optimally to two orthogonal orientations of the phase shifts (von der Heydt & Peterhans, 1989; Fig. 5A & Fig. 10). One preferred orientation was the same as that of the grating, likely reflecting nonlinear processing, while the other probably resulted from linear responses to the line terminations. Thus, using only fixed (very thin) lines may not suffice to avoid luminance-edge responses, since it is not the absolute width but

rather the width relative to the neuron's luminance resolution that will determine whether the local luminance contrast can drive a neural response.

Whether neurons in primary visual cortex can process abutting gratings in a similar way has been controversial. von der Heydt and Peterhans (1989) reported that 1 out of 60 sampled primate V1 neurons responded to abutting grating contours, while Sheth et al. (1996) found this portion to be around 8–9% in cat A17. Since the neurons from both of these studies had similar orientation preferences for abutting gratings and luminance gratings, they are quite likely to reflect nonlinear processing. In contrast, Ramsden et al. (2001) found that the orientation map was reversed for abutting gratings compared to luminance gratings. Their single-unit data also demonstrated different orientation preferences for the two stimuli. Considering that orientation preference of linear responses does not necessarily correlate with that of gratings (e.g. Fig. 1F), their results are likely to reflect orientation tuning for luminance contrast at line terminations rather than the genuine nonlinear processing of illusory contours.

Relation to previous studies

Several studies have shown that many A18 neurons respond to contrast-modulated gratings with a characteristic tuning to high carrier spatial frequencies that are outside the neurons' luminance passband (e.g. Zhou & Baker, 1993) and with varying degrees of selectivity to carrier orientation (Mareschal & Baker, 1998). These neurons were also selective for similar orientations and movement directions for envelopes and luminance gratings (Mareschal & Baker, 1998). The similarity of these properties to those described here for nonlinear responses to abutting gratings suggests that both might be mediated by the same neurons, and indeed by the same mechanism (Song & Baker, 2004a,b), though this possibility has yet to be explored in detail.

Mechanisms of abutting grating responses

How might one model these two kinds of abutting grating responses? First, our results suggest that many A18 neurons process abutting gratings in a "two-stream" mode, since a single neuron can respond to abutting gratings through either a linear summation or a nonlinear mechanism. In this scheme, abutting gratings of low carrier spatial frequency as well as luminance gratings are processed through a conventional linear filter (F_0) selective for orientation and a low spatial frequency (upper pathway in Fig. 16A). This linear processing of abutting gratings depends on the carrier phase, which, together with carrier spatial frequency, determines the local luminance energy. However, abutting gratings composed of sufficiently high carrier spatial frequencies are processed *via* a distinct pathway (lower pathway in Fig. 16A) that is highly nonlinear.

One candidate for this nonlinear processing is the FRF model (Chubb & Sperling, 1988; Malik & Perona, 1990; Baker, 1999; Wilson, 1999). In this model (Fig. 16B), the early filter (F_1) has a small spatial scale selective for high carrier spatial frequencies that are well beyond the F_0 passband. Filter F_1 is also selective for orientation, narrowly in some neurons (Figs. 14A & B) and broadly in others (Figs. 14C & D). The broad carrier orientation tuning may reflect a pooling of various orientations (Landy & Bergen, 1991; Mareschal & Baker, 1999). Notice that F_1 will not respond at the phase shifts, since the light and dark parts of the stimulus cancel out within excitatory and inhibitory zones of F_1 . In

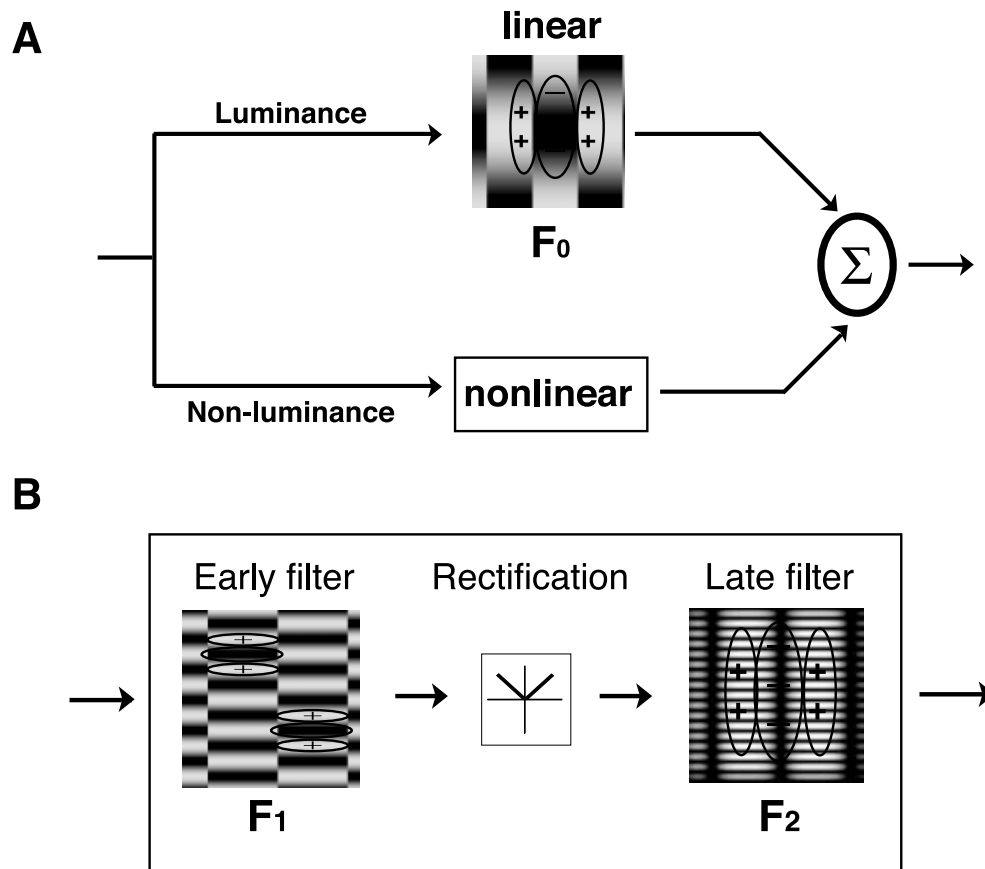


Fig. 16. A schematic model accounting for abutting grating responses. A, a two-stream processing scheme, in which linear and nonlinear responses are mediated by separate, parallel pathways. The top pathway is a classic linear spatial filter (F_0), which mediates selectivity to conventional sinewave gratings as well as abutting gratings with low carrier spatial frequencies. The latter case is illustrated by an abutting grating stimulus superimposed on a cartoon linear receptive field (filter). The bottom pathway mediates nonlinear processing of abutting gratings with high carrier spatial frequency (ICs). B, possible implementation of the nonlinear pathway, as an FRF cascade. The early filters (F_1) are shown overlaid on an IC stimulus, demonstrating how they could mediate spatial frequency and orientation selectivity for the component (carrier) gratings. Although demonstrated as a single orientation channel, F_1 could also be a pooling of various orientations. The rectification pools both positive and negative early filter responses. The late filter (F_2) is shown superimposed on the full-wave rectified F_1 responses to illustrate its selectivity for the envelope spatial frequency and orientation of ICs.

Fig. 16B, the late-stage, coarser scale filter (F_2) is shown superimposed on the F_1 filtered and full-wave rectified stimulus to illustrate its selectivity for the envelope spatial frequency and orientation. Compared to F_0 in the linear pathway, F_2 has about the same orientation preference, and a consistent preferred direction, but a typically somewhat coarser spatial preference. An essential nonlinear operation, such as rectification or squaring, is required to connect the two different linear filters (F_1 and F_2) so that the positive and negative outputs of F_1 are not canceled out by the coarse-scale filtering of F_2 . Notice that the optimal carrier orientation is not necessarily orthogonal to the global filters (F_2), as sometimes suggested (Wilson & Richards, 1992; Soriano et al., 1996). Altogether, the FRF mechanism smooths out the fine local pattern (carrier) and captures the global information (envelope).

Alternative models for nonlinear processing of abutting gratings involve at least two sets of end-stopped cells responding to the line terminations on the opposite sides of the contour (Fig. 1B; Grossberg & Mingolla, 1985; von der Heydt & Peterhans, 1989). Signals from appropriate combinations of these end-stopped cells converge on a single neuron that responds selectively to the ICs'

orientation. Notice that some sort of nonlinear operation, either end inhibition in the end-stopped model or rectification in the energy model (FRF), is essential to both schemes.

Our present data do not necessarily exclude the possibility that a mechanism based on classic end-stopped cells could signal the ICs. However, our findings would be more readily understood in the FRF scheme, since the response dependence on orientation and spatial frequency of carrier and envelope is more naturally predicted from the properties of the linear filters (F_1 and F_2). The FRF model is more parsimonious, since it does not require an additional population of end-stopped cells. Furthermore, such an end-stopped type of mechanism would have limited functional utility because of its dependence on logical combinations of particular local "features" (oriented terminators). Since the FRF model responds to gradients of stimulus energy, regardless of the type of pattern containing them, it would have the flexibility to respond to other types of non-luminance-defined stimuli (Prins & Kingdom, 2003). Consistent with this idea, such FRF-type schemes have also been proposed to mediate visual perception of stimuli that lack luminance contrast in psychophysics studies, such as texture segrega-

tion based on differences in orientation (Malik & Perona, 1990; Bergen & Landy, 1991; Landy & Bergen, 1991; Kingdom et al., 1995, 2003), contrast (Sutter & Graham, 1995), spatial frequency (Arsenault et al., 1999), or element arrangement (Graham et al., 1992; Sutter & Graham, 1995; Graham & Sutter, 1998). FRF models have also been proposed to mediate psychophysical detection of moving contrast-modulated patterns (Chubb & Sperling, 1988) and moving glass patterns (Wilson et al., 1997; Wilson & Wilkinson, 1998). It is also predictable from the FRF models, but not necessarily from the end-stopped models, that single early cortical visual neurons could respond selectively to a variety of non-luminance-defined contours (Song & Baker, 2004a,b).

Acknowledgments

This work was supported by the Canadian Institutes of Health Research grant MA-9685 to C.L.B. We thank Rhone-Poulenc Rorer for donation of Gallamine triethiodide. We thank Steven Dakin for contribution to the stimulus software. We thank Lynda Domazet, Aaron Johnson, and Chang'an Zhan for assistance with the experiments.

References

- ALBRIGHT, T.D. (1992). Form-cue invariant motion processing in primate visual cortex. *Science* **225**, 1141–1143.
- ARSENAULT, S.A., WILKINSON, F. & KINGDOM, F.A.A. (1999). Modulation frequency and orientation tuning of second-order texture mechanisms. *Journal of the Optical Society of America A* **16**, 427–435.
- BAKER, C.L. (1999). Central neural mechanisms for detecting second-order motion. *Current Opinion in Neurobiology* **9**, 461–466.
- BERGEN, J.R. & LANDY, M.S. (1991). Computational modelling of visual texture segregation. In *Computational Models of Visual Processing*, ed. LANDY, M.S. & MOVSHON, J.A., pp. 253–271. Cambridge, Massachusetts: MIT Press.
- BRAINARD, D.H. (1997). The Psychophysics Toolbox. *Spatial Vision* **10**, 433–436.
- CHUBB, C. & SPERLING, G. (1988). Drift-balanced random stimuli: A general basis for studying non-Fourier motion perception. *Journal of the Optical Society of America A* **5**, 1986–2007.
- FERSTER, D. & JAGADEESH, B. (1991). Nonlinearity of spatial summation in simple cells of areas 17 and 18 of cat visual cortex. *Journal of Neurophysiology* **66**, 1667–1679.
- GRAHAM, N., BECK, J. & SUTTER, A. (1992). Nonlinear processes in spatial-frequency channel models of perceived segregation: Effects of sign and amount of contrast. *Vision Research* **32**, 719–743.
- GRAHAM, N. & SUTTER, A. (1998). Spatial summation in simple (Fourier) and complex (no-Fourier) texture channels. *Vision Research* **38**, 231–257.
- GROSOFF, D.H., SHAPLEY, R.M., HAWKEN, M.J. (1993). Macaque V1 neurons can signal “illusory” contours. *Nature* **365**, 550–552.
- GROSSBERG, S. & MINGOLLA, E. (1985). Neural dynamics of form perception: Boundary completion, illusory figures, and neon color spreading. *Psychological Review* **92**, 173–211.
- HORRIDGE, G.A., ZHANG, S.W. & O’CARROLL, D. (1992). Insect perception of illusory contours. *Philosophical Transactions of the Royal Society B (London)* **337**, 59–64.
- HUBEL, D.H. & WIESEL, T.N. (1962). Receptive fields, binocular interaction and functional architecture in the cat’s visual cortex. *Journal of Physiology* **160**, 106–154.
- JONES, J.P. & PALMER, L.A. (1987). The two-dimensional spatial structure of simple receptive fields in cat striate cortex. *Journal of Neurophysiology* **58**, 1187–1211.
- KENNEDY, J.M. (1978). Illusory contours and the ends of lines. *Perception* **7**, 605–607.
- KINGDOM, F.A.A., KEEBLE, D. & MOULDEN, B. (1995). Sensitivity to orientation modulation in micropattern-based textures. *Vision Research* **35**, 79–91.
- KINGDOM, F.A.A., PRINS, N. & HAYES, A. (2003). Mechanism independence for texture-modulation detection is consistent with a filter-rectify-filter mechanism. *Visual Neuroscience* **20**, 65–76.
- LANDY, M.S. & BERGEN, J.R. (1991). Texture segregation and orientation gradient. *Vision Research* **31**, 679–691.
- LEVENTHAL, A.G., WANG, Y., SCHMOLESKY, M.T. & ZHOU, Y. (1998). Neural correlates of boundary perception. *Visual Neuroscience* **15**, 1107–1118.
- MALIK, J. & PERONA, P. (1990). Preattentive texture discrimination with early vision mechanisms. *Journal of the Optical Society of America A* **7**, 923–932.
- MARESCAL, I. & BAKER, C.L., JR. (1998). A cortical locus for the processing of contrast-defined contours. *Nature Neuroscience* **1**, 150–154.
- MARESCAL, I. & BAKER, C.L., JR. (1999). Cortical processing of second-order motion. *Visual Neuroscience* **16**, 527–540.
- MARIDA, K.V. (1972). *Statistics of Directional Data*. New York: Academic Press.
- MOVSHON, J.A., THOMPSON, I.D. & TOLHURST, D.J. (1978). Spatial and temporal contrast sensitivity of neurones in areas 17 and 18 of the cat’s visual cortex. *Journal of Physiology* **283**, 101–120.
- NIEDER, A. (2002). Seeing more than meets the eye: Processing of illusory contours in animals. *Journal of Comparative Physiology* **188**, 249–260.
- NIEDER, A. & WAGNER, H. (1999). Perception and neuronal coding of subjective contours in the owl. *Nature Neuroscience* **2**, 660–663.
- PEI, X., VIDYASAGAR, T.R., VOLGUSHEV, M. & CREUTZFELDT, O.D. (1994). Receptive field analysis and orientation selectivity of postsynaptic potentials of simple cells in cat visual cortex. *Journal of Neuroscience* **14**, 7130–7140.
- PEIRCE, J.W. & LENNIE, P. (2002) ‘Illusory contour’ responses in early visual cortex explained by linear mechanisms. Program no. 456.4. 2002 Abstract Viewer/Itinerary Planner. Washington, DC: Society for Neuroscience. Online.
- PELLI, D.G. (1997). The VideoToolbox software for visual psychophysics: Transforming numbers into movies. *Spatial Vision* **10**, 437–442.
- PESSOA, L., THOMPSON, E. & NOE, A. (1998). Finding out about filling-in: A guide to perceptual completion for visual science and the philosophy of perception. *Behavioral and Brain Sciences* **21**, 723–748.
- PETERHANS, E. (1997). Functional organization of Area V2 in the awake monkey. In *Cerebral Cortex*, ed. ROCKLAND, K.S., KAAS, J.H. & PETERS, A., pp. 335–357. New York: Plenum Press.
- PRINS, N. & KINGDOM, F.A.A. (2003). Detection and discrimination of texture modulations defined by orientation, frequency and contrast. *Journal of the Optical Society of America A* **20**, 401–410.
- RAMSDEN, B.M., HUNG, C.P. & ROE, A.W. (2001). Real and illusory contour processing in area V1 of the primate: A cortical balancing act. *Cerebral Cortex* **11**, 648–665.
- REDIES, C., CROOK, J.M. & CREUTZFELDT, O.D. (1986). Neuronal responses to borders with and without luminance gradients in cat visual cortex and dorsal lateral geniculate nucleus. *Experimental Brain Research* **61**, 469–481.
- RINGACH, D.L., HAWKEN, M.J. & SHAPLEY, R. (1997). Dynamics of orientation tuning in macaque primary visual cortex. *Nature* **387**, 281–284.
- SHETH, B.R., SHARMA, J., RAO, S.C. & SUR, M. (1996). Orientation maps of subjective contours in visual cortex. *Science* **274**, 2110–2115.
- SKOTTUN, B.C. (1994). Illusory contours and linear filters. *Experimental Brain Research* **100**, 360–364.
- SKOTTUN, B.C., DE VALOIS, R.L., GROSOFF, D.H., MOVSHON, J.A., ALBRECHT, D.G. & BONDS, A.B. (1991). Classifying simple and complex cells on the basis of response modulation. *Vision Research* **31**, 1079–1086.
- SONG, Y. & BAKER, C. L. (2004a). A common mechanism underlying neuronal processing of contrast envelopes and illusory contours [Abstract]. *Journal of Vision* **4**, 66a, <http://journalofvision.org/4/8/66/>, doi:10.1167/4.8.66.
- SONG, Y. & BAKER, C.L. (2004b). A cortical locus for form-cue invariant boundary perception. Program no. 986.1. Abstract Viewer/Itinerary Planner. Washington, DC: Society for Neuroscience. Online.
- SORIANO, M., SPILLMANN, L. & BACH, M. (1996). The abutting grating illusion. *Vision Research* **36**, 109–116.
- SPITZER, H. & HOCHSTEIN, S. (1985a). A complex cell receptive field model. *Journal of Neurophysiology* **53**, 1281–1301.
- SPITZER, H. & HOCHSTEIN, S. (1985b). Simple- and complex-cell response dependences on stimulation parameters. *Journal of Neurophysiology* **53**, 1244–1265.
- SUTTER, A. & GRAHAM, N. (1995). Investigating simple and complex mechanisms in texture segregation using speed-accuracy trade-off method. *Vision Research* **35**, 2825–2843.

- VON DER HEYDT, R. & PETERHANS, E. (1989). Mechanisms of contour perception in monkey visual cortex. I. Lines of pattern discontinuity. *Journal of Neuroscience* **9**, 1731–1748.
- VON DER HEYDT, R., PETERHANS, E. & BAUMGARTNER, G. (1984). Illusory contours and cortical neuron responses. *Science* **224**, 1260–1262.
- WESTHEIMER, G. & LI, W. (1996). Classifying illusory contours by means of orientation discrimination. *Journal of Neurophysiology* **75**, 523–537.
- WILSON, H.R. (1999). Non-Fourier cortical processes in texture, form, and motion perception. In *Cerebral Cortex: Models of Cortical Circuitry*, ed. ULINSKI, P.S. & JONES, E.G., pp. 445–477. New York: Kluwer Academic/Plenum.
- WILSON, H.R. & RICHARDS, W.A. (1992). Curvature and separation discrimination at texture boundaries. *Journal of the Optical Society of America A* **9**, 1653–1662.
- WILSON, H.R. & WILKINSON, F. (1998). Detection of global structure in glass patterns: Implications for form vision. *Vision Research* **38**, 2933–2947.
- WILSON, H.R., WILKINSON, F. & ASAAD, W. (1997). Concentric orientation summation in human form vision. *Vision Research* **37**, 2325–2330.
- ZHAN, C. & BAKER, C.L., JR. (2004). Critical spatial frequencies for illusory contour processing in early visual cortex. Program no. 986.2. Abstract Viewer/Itinerary Planner. Washington, DC: Society for Neuroscience. Online.
- ZHAN, C.A. & BAKER, C.L., JR. (2006). Boundary cue invariance in cortical orientation maps. *Cerebral Cortex*, in press.
- ZHOU, Y.F., JIA, F., TAO, H.Y. & SHOU, T.D. (2001). The responses to illusory contours of neurons in cortex areas 17 and 18 of the cats. *Science in China Series C-Life Sciences* **44**, 136–145.
- ZHOU, Y.X. & BAKER, C.L., JR. (1993). A processing stream in mammalian visual cortex neurons for non-Fourier responses. *Science* **261**, 98–101.
- ZHOU, Y.X. & BAKER, C.L., JR. (1996). Spatial properties of envelope-responsive cells in area 17 and 18 neurons of the cat. *Journal of Neurophysiology* **75**, 1038–1050.